Biochemical Evidence for Multiple Dimeric States of the *Sinorhizobium meliloti* DctD Receiver Domain†

Sungdae Park,‡ Hong Zhang,‡ A. Daniel Jones,§ and B. Tracy Nixon*,‡

Department of Biochemistry and Molecular Biology and Department of Chemistry, The Pennsylvania State University, University Park, Pennsylvania 16802

Received April 23, 2002; Revised Manuscript Received July 9, 2002

ABSTRACT: X-ray crystal structures suggest very different dimeric states for the inactive and active forms of the two-component receiver domain of *Sinorhizobium meliloti* DctD, a σ^{54}-dependent AAA+ ATPase. Moreover, the receiver domain in crystals grown from unphosphorylated protein is refractory to phosphorylation whereas solution protein is fully phosphorylatable, and equilibrium analytical ultracentrifugation data are consistent with solution dimers for both phosphorylated and unphosphorylated forms of the protein. Here we report biochemical data consistent with the presence of multiple dimeric conformations in the inactive and active states, and evidence for significant change in the dimeric state upon activation by phosphorylation or binding of Mg^{2+} and BeF_3^-.

The *dct* genes of *Sinorhizobium meliloti* and *Rhizobium leguminosarum* are essential for the bacteria to use 4-carbon dicarboxylic acids as a sole carbon and energy source and to fix nitrogen as endosymbionts of their respective host plants, Alfalfa and pea (*1*−*3*, and references cited therein). The *dctA* gene encodes a transport protein specific for the organic acids succinate, fumarate, and malate. Expression of *dctA* is stimulated by the external presence of these compounds via the two-component signal transduction proteins DctB and DctD. DctB is a histidine kinase sensor protein, and DctD, the cognate response regulator, is a σ^{54}-dependent, enhancer binding protein. Three domains mediate the actions of DctD. The first 125 residues form an N-terminal 2-component receiver domain. This domain regulates the activity of a central transcription activation domain, comprised of residues 148−384. The latter domain exhibits similarity to members of the AAA+ ATPase[1] superfamily (*4*), and it uses purine nucleotide hydrolysis to enable the σ^{54}-form of RNA polymerase to melt promoter regions and thus to initiate transcription (*5*). A C-terminal DNA binding domain gives specificity to the DctD protein, cooperatively binding to tandem sites between −100 and −150 base pairs upstream of the *dctA* promoter (*5*−*8*).

Previously we showed that the N-terminal receiver domain (N) of DctD and the adjacent linker (L) joining it to the AAA+ ATPase domain form a stable dimer in solution when expressed as an isolated fragment (hereafter referred to as DctDNL; *9*). The crystal structure of DctDNL revealed a dimeric structure novel for two-component receiver domains. Random amino acid substitutions that derepressed the AAA+ ATPase domain of DctD mapped almost exclusively to the receiver domain or linker region with 65% occurring in residues directly involved in subunit−subunit contacts of the dimer interface. Though two of these substitutions were shown to reduce dimer stability 10−20-fold, suggesting that activation might occur via monomerization, the protein was still a stable dimer in solution when excess carbamyl phosphate and Mg^{2+} were used to maintain DctDNL in its phosphorylated state. It had previously been shown that full-length DctD protein is a stable dimer at nanomolar concentrations (*8*). Other studies indicate that AAA+ ATPase domains are typically hexameric (reviewed in *4* and *10*). We thus suggested that the unphosphorylated receiver domain and linker form a ground-state dimeric structure that represses an intrinsic ability of the DctD AAA+ ATPase domain to assemble to an active enzyme, and that phosphorylation activates by stabilizing an altered dimeric state that does not repress the ATPase domain.

We are presenting continued study of two-component signal transduction in the DctDNL protein in three parts. Elsewhere we report crystal structures for an alternative off-state dimer of DctDNL (Meyer et al., unpublished results) and of Mg^{2+}-BeF_3^- -bound DctDNL that also bears the amino acid substitution E121K (*11*). Binding of BeF_3^- to the conserved aspartate's carboxylic acid group mimics its phosphorylation and thus triggers signal transduction in DctD and other two-component response regulators (*9*, *12*). The E121K substitution weakens the DctDNL dimeric state about

† Supported by NSF Grant MCB-9727745 (to B.T.N.) and National Center for Research Resources Grants RR11264 and RR11318. The analytical ultracentrifuge was funded by the National Center for Research Resources (Grant RR11264). The mass spectrometer was purchased with funds from NIH Grant RR11318 (to A.D.J.).

* Corresponding author. Telephone: (814) 865-1554. Telefax: (814) 863-7024. Email: btn1@psu.edu.

‡ Department of Biochemistry and Molecular Biology.

§ Department of Chemistry.

[1] Abbreviations: AAA+ ATPase, cellular activity associated ATPases; CD, circular dichroism; DctDNL, protein fragment of DctD residues 2−143 followed by a His tag, containing the N-terminal two-component receiver domain and the linker that joins it to the central AAA+ ATPase domain; DctDNL-P, phosphorylated DctDNL; ϵ287nm, molar extinction coefficient for 287 nm light; GuHCl, guanidine hydrochloride; HSQC spectra, heteronuclear single quantum coherence spectra; Mg^{2+}-BeF_3^- -DctDNL(E121K), fragment DctDNL bearing the amino acid substitution E121K bound to magnesium and beryllofluoride; NMR, nuclear magnetic resonance; RMSD, root-mean-square deviation.

10.1021/bi0260031 CCC: $22.00
Published on Web 08/15/2002

20-fold, partially derepresses the ATPase activity, and makes the full-length protein more easily activated by phosphorylation or by binding Mg^{2+} and BeF_3^-. The crystal lattice for Mg^{2+}-BeF_3^- -DctDNL(E121K) contains multiple 'dimers' in which monomers are packed very differently from those in the off-state dimer. One of these potential dimers seems most likely to be biologically relevant because it has a buried surface area sufficient to sustain a typical dimer of 34 kDa (*13*) and is symmetric, and its interface involves contact between remodeled helix α4 and strand *β*5, now known to be the signaling surface in a few two-component receiver domains (for examples, see *11*, *14*−*18*). Here we report solution studies showing that although phosphorylation or binding BeF_3^- does not appear to alter the secondary structure of DctDNL, such activation does decrease sedimentation velocity, increase fluorescence anisotropy, dramatically alter thermal stability, and alters the environment of many residues, including residue Y100 of the 'off-state' dimer interface. Together these observations are consistent with phosphorylation stabilizing a substantially different dimeric form of DctDNL than the unphosphorylated form. Minimally, the phosphorylated form fails to repress the AAA+ ATPase domain, but it could also increase the activity of this domain. The results demonstrate that subtle changes in protein structure can induce important preferences in multimerization which in turn dramatically alters physical characteristics.

MATERIALS AND METHODS

Protein. DctDNL protein was expressed in cultures of *E. coli* strain BL21(DE3) pLysS (Novagen) and purified to >99% homogeneity using cobalt-affinity chromatography (Qiagen) followed by Mono-Q ion exchange chromatography (Amersham/Pharmacia). For NMR studies, uniform labeling was achieved using M9 minimal medium supplemented with [^{15}N]ammonium chloride (Aldrich) as the sole nitrogen source. For selective labeling, [^{15}N]tyrosine (0.085 g/L; Aldrich) was added to a defined medium for growing strain CT16 bearing pLysS and the DctDNL expression plasmid. Strain CT16 (*19*), kindly provided by D. Waugh (Roche Research Center, Nutley, NJ), is a tyrosine auxotroph of its parent, BL21(DE3). To prepare 1 L of the defined medium, the following were autoclaved in 940 mL of water: alanine (0.5 g), arginine (0.4 g), aspartic acid (0.4 g), asparagine (0.4 g), cysteine (0.1 g), glutamic acid (0.65 g), glutamine (0.4 g), glycine (0.55 g), histidine (0.1 g), isoleucine (0.23 g), leucine (0.23 g), lysine (0.42 g), methionine (0.25 g), phenylalanine (0.13 g), proline (0.1 g), serine (2.1 g), threonine (0.23 g), valine (0.23 g), adenine (0.5 g), guanosine (0.65 g), thymine (0.2 g), uracil (0.5 g), cytosine (0.2 g), sodium acetate (1.5 g), succinic acid (1.5 g), ammonium chloride (0.5 g), sodium hydroxide (0.85 g), and potassium phosphate dibasic (10.5 g). To this were added 50 mL of 40% glucose, 4 mL of 1 M magnesium sulfate, 1 mL of 10 mM ferric chloride, and 10 mL containing: 2 mg each of calcium chloride, zinc sulfate, and magnesium sulfate; 50 mg each of tryptophan, thiamin, and niacin; 1 mg of biotin; and 100 mg of ampicillin.

Circular Dichroism, Fluorescence, and Absorbance Spectroscopy. Unless otherwise noted, the conditions were 7 mM potassium phosphate (pH 6.89) and 25 °C, with varying presence of magnesium chloride (100 mM), carbamyl phosphate (100 mM; Sigma Chemical Co.), beryllium chloride (5 mM; Aldrich), sodium chloride or sodium fluoride (49 mM; Sigma Chemical Co.). Fluorescence data were collected on an AVIV model ATF-105/305 differential/ratio spectrofluorometer; circular dichroism data were collected on an AVIV 62DS spectrophotometer; and absorbance data were collected on an AVIV model 118-UV-VIS spectrophotometer. The equilibrium unfolding data shown in Figure 2 were collected using an automated titrator. Longer time between readings verified that equilibrium had been reached in the data presented. The time course for phosphorylation-induced changes in equilibrium fluorescence anisotropy, defined as $r = (I_{VV} - GI_{VH})/(I_{VV} - 2GI_{VH})$ with G being an measured instrument correction factor, was analyzed using Savuka software (kindly provided by O. Bilsel, Department of Biochemistry and Molecular Pharmacology, University of Massachusetts Medical School, Worcester, MA) by nonlinear regression for a two-species model that included quantum yield parameters for each species. Excitation was at 280 nm, and emission at 321 nm. The absorbance data shown in Figure 7 had to be performed manually, with a shutter blocking light except during readings for sample undisturbed in the holder, as continuous light showed a biphasic transition consisting first of an increasing signal followed by a decreasing one. The increasing signal was associated with solutions lacking protein, but containing $MgCl_2$ and carbamyl phosphate. The signal for these observations was ∼0.1 OD_{287nm}, and the change was well within the error limits of the instrument, which over 2 h prior to the above measurements typically gave an average signal for buffer containing $MgCl_2$ of 0.04688 with a standard deviation of 0.00019.

Sedimentation Velocity. Optical density data were collected at 237 nm using an An60 rotor in an XL-I analytical ultracentrifuge (Beckman Coulter, Inc.) using conventional sectored cells. Protein, present at 38 *μ*M dimer, giving a loading OD_{237nm} of 1.08, was preincubated 2 h at 25 °C in sodium phosphate buffer (7 mM, pH 6.89) containing $MgCl_2$ (100 mM), carbamyl phosphate (100 mM), or both. After mixing, but prior to incubation, the samples were filtered through 0.1 *μ*m filters to remove a small amount of aggregate that accompanied mixing with the high-salt solutions. After incubation, samples were equilibrated to 20 °C for 1 h, and then centrifuged at 60 000 rpm. Fifty radial scans were collected between 45 min and 2 h after initiating the run for van Holde−Weischet analysis (*20*) using the program UltrascanII (B. Demeler, The University of Texas Health Science Center, San Antonia, TX). To minimize the time between scans, samples were spun in separate experiments, and single readings were taken at each radial position.

Mass Spectrometry. Protein samples were desalted into 0.1% formic acid using an HR5 desalting column and FPLC system (Amersham/Pharmacia). Immediately after elution, desalted protein was cooled to −80 °C until it was thawed and analyzed on a Perseptive Mariner time-of-flight instrument with electrospray interface. The mass spectrometer ion source was connected to a Hewlett-Packard 1100 HPLC pump, with samples being delivered directly using flow injection analysis. Zero-charge-state spectra were calculated from the multiply charged peaks in the spectra using Perseptive BioSpec Data Explorer software, and the relevant

peak heights were measured for calculating the percent of protein in native, phosphorylated, or carbamylated forms.

^{1}H-^{15}N HSQC Spectroscopy. Heteronuclear single quantum coherence spectra data were collected using a Bruker DRX-600 spectrometer and analyzed using Felix software (Biosym Technologies, San Diego). For unmodified DctDNL, 64 transients were collected at 800 μM protein (monomer equivalents) in water containing 50 mM $MgCl_2$, pH 6.8, giving ~110 peaks. To prepare BeF_3^- -bound protein, the same sample was diluted to 700 μM upon adding 4 mM $BeCl_2$ and 40 mM NaF, and adjusting the pH to 6.8 with sodium hydroxide. About 15% of the protein precipitated, which was removed by centrifugation followed by passing the supernatant through a 0.1 μm filter (Whatman). Data were collected for 128 transients, giving ~170 peaks. For work with selectively labeled protein with and without phosphorylation, protein in 5 mM phosphate buffer (pH 7.0) containing 67 mM $MgCl_2$ was examined, and then 100 mM carbamyl phosphate was added to begin the phosphorylation reaction. After briefly spinning the sample, data were collected over 32, 64, or 128 transients at various times and temperatures. Aliquots of a reaction performed in parallel were subjected to electrospray mass spectrometry analysis to follow the time course of phosphorylation, typically reaching 90% within 90−120 min, with 45% phosphorylation being obtained in 20 or 30 min at 25 and 15 °C, respectively.

RESULTS

The crystal structures of DctDNL and Mg^{2+}-BeF_3^- -DctDNL(E121K) suggest that little change occurs in secondary structure upon phosphorylation of this receiver domain. CD spectroscopy was used to test for such changes in solution. Phosphorylation caused a small decrease in ellipticity corresponding to helical components (Figure 1A). By monitoring the signal at 221 nm, this small change was seen to develop in parallel with the phosphorylation reaction (Figure 1B). A larger, reversible increase in ellipticity at 221 nm was observed when DctDNL or DctDNL-P was cooled from 25 to 5 °C (Figure 1B).

Even though the crystal structures suggest small changes in secondary structure when the receiver domain is activated, they indicate dramatic changes occur in its multimerization properties. Thermal denaturation experiments showed a dramatic change in the overall stability of the DctDNL protein when it was activated using BeF_3^- (Figure 2A; these experiments were not performed using carbamyl phosphate to phosphorylate the DctDNL protein because it was anticipated that incubations at elevated temperatures would increase uncatalyzed hydrolysis of carbamyl phosphate, both diminishing the phosphorylation reaction and increasing a carbamylation side reaction). The unmodified protein was found to retain significant secondary structure after a transition centered at about 64 °C. This stability was lost when the melting experiment was conducted in the presence of BeF_3^-. In the presence of BeF_3^-, there was also an apparent transition between 20 and 40 °C that was not evident in its absence. Even though protein was soluble at the end of both of the unfolding reactions, cooling samples led to aggregation rather than refolding. In contrast to these results, unfolding of unphosphorylated protein with guanidine hydrochloride did not lead to a metastable state, and with the exception of a complex but subtle event occurring between

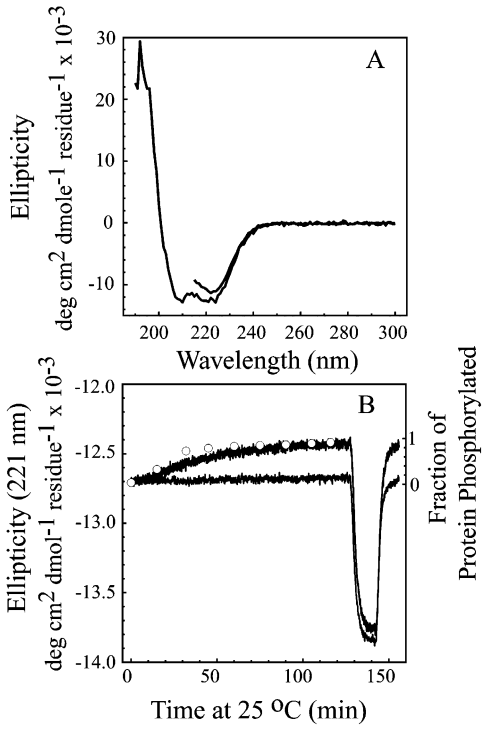

FIGURE 1: Changes in circular dichroism upon phosphorylation of DctDNL. (A) CD spectra are shown for 4.5 μM DctDNL dimer in sodium phosphate buffer (7 mM, pH 6.89; gray line) or the same incubated for 2 h at 25 °C together with $MgCl_2$ and carbamyl phosphate (100 mM each; black line; the absorbance due to the relatively high concentrations of $MgCl_2$ and carbamyl phosphate prevented measuring below 215 nm). (B) Ellipticity at 221 nm is plotted vs time for DctDNL incubated in the absence (gray line) or presence of $MgCl_2$ and carbamyl phosphate (black line). At 120 min, the temperature was quickly changed from 25 to 5 °C, and then raised back to 25 °C at 140 min. Also shown is the 2 h time course for phosphorylation (right *y*-axis, ○) determined by mass spectrometry.

0 and 1 M GuHCl, this denaturation was largely reversible (Figure 2B). In similar chemical unfolding reactions, fluorescence anisotropy increased between 0 and 1.4 M GuHCl, after which it decreased to a new baseline (Figure 2C). This signal monitors the local environment of the single tyrosine in DctDNL, residue Y100, as well as the global rotational tumbling of the assembled form(s) of the protein.

Analytical ultracentrifugation experiments can also provide information about structural changes in the solution states of DctDNL and DctDNL-P. Prior equilibrium studies showed that both states are dimeric (*9*). Van Holde−Weishet analysis of sedimentation velocity data showed no change when DctDNL was spun in the ultracentrifuge in the presence of Mg^{2+} or carbamyl phosphate, but the sedimentation coefficient decreased from 2.65 $S_{W,20}$ to 2.40 $S_{W,20}$ when both reagents were combined to phosphorylate the protein. During the sedimentation experiment, 95% of the protein was phosphorylated, and by the end of the experiment, 10% was carbamylated. Plots of the boundary fraction versus sedimentation coefficient (Figure 3A) give a single vertical line for each sample, suggesting (but not proving) homogeneity in the protein samples (*21*). Changes in fluorescence anisotropy can also reflect changes in shape. Fluorescence anisotropy of DctDNL was seen to increase in parallel with the phosphorylation reaction (Figure 3B).

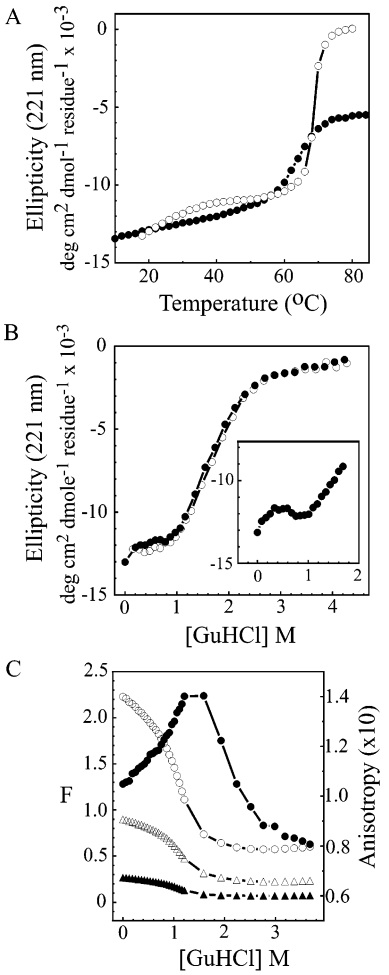

FIGURE 2: Denaturation profiles. (A) Ellipticity at 221 nm for 4.5 μM DctDNL dimer in phosphate buffer plus 67 mM $MgCl_2$, 7 mM $BeCl_2$, and 49 mM NaCl (●), or the same with NaCl replaced by NaF (○) at various temperatures. (B) Ellipticity at 221 nm for 4.5 μM DctDNL dimer in the absence of phosphorylating reagents, equilibrated with increasing (●) or decreasing (○) amounts of GuHCl; the inset shows smaller increments in the titration. (C) Fluorescence (total, ○; I_{VV}, △; I_{VH}, ▲) and anisotropy (●) changes during titration of 4.5 μM DctDNL dimer with GuHCl.

NMR chemical shift data are exquisitely sensitive to changes in local chemical environments, and line-broadening of spectral peaks can reveal the presence of equilibria between multiple species. ^{15}N-^{1}H heteronuclear single quantum coherence spectra of unphosphorylated and phosphorylated or BeF_3^- -bound protein showed phosphorylation-related differences in chemical shifts for a majority of the backbone amide nitrogen atoms (Figure 4). Residue Y100 is a crucial component of the 'off-state' dimer interface (*9*) wherein the hydroxyl group hydrogen-bonds with its counterpart in the other subunit (see Figure 5A); it is also the only tyrosine residue in the DctDNL protein. By using [^{15}N]-tyrosine to specifically label the backbone amide nitrogen of Y100, it was possible to assign cross-correlation peaks for this residue. Comparing peaks for inactive and active protein revealed phosphorylation-dependent changes in the chemical environment of the backbone nitrogen of this dimer-interface residue (Figure 5B). A single HSQC peak was observed for unphosphorylated protein in 5 mM phosphate buffer (pH 7.0) at 8.5 ppm on the proton axis and at 120 ppm on the nitrogen axis. The intensity of this peak was

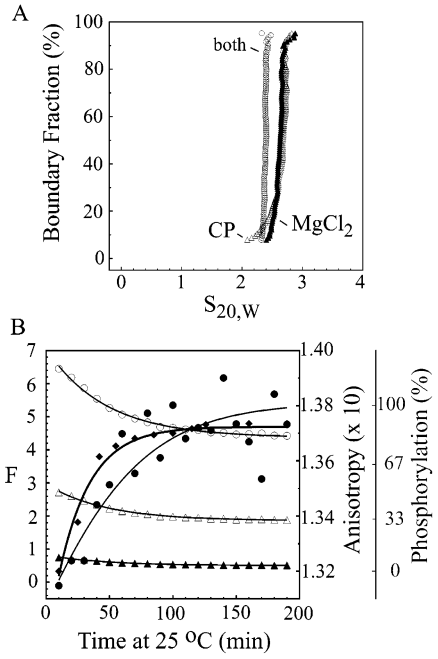

FIGURE 3: Sedimentation velocity and fluorescence anisotropy changes upon phosphorylation. (A) van Holde−Weischet analysis of sedimentation velocity data for 38 μM dimer (OD_{237nm} = 1.08) preincubated 2 h at 25 °C in phosphate buffer (7 mM, pH 6.89) containing $MgCl_2$ (100 mM, ▲), carbamyl phosphate (100 mM, △), or both (○), equilibrated to 20 °C for 1 h, and then spun at 60 000 rpm. (B) Fluorescence (total, ○; I_{VV}, △; I_{VH}, ▲) and anisotropy (●) changes during phosphorylation of DctDNL [4.5 μM dimer in phosphate buffer (7 mM, pH 6.89) containing $MgCl_2$ (100 mM) and carbamyl phosphate (100 mM) at 25 °C]. The solid curves are the best-fit solutions to a two-species model with the following parameters: $r_A = 0.1307 \pm 0.0050$; $r_B = 0.138 \pm 0.0031$; $q_A = 7.05 \pm 0.064$; $q_B = 4.37 \pm 0.025$; $\tau = 46.5 \pm 1.41$ min; $G = 2.489$. Also shown (◆) is the time course for phosphorylation, with the best-fit solution to a single-exponential model (amplitude = 89.4 ± 1.2%, time constant τ = 26.8 ± 1.9 min). At 3 h, 15% of the phosphorylated protein was modified with a single carbamylation (not shown).

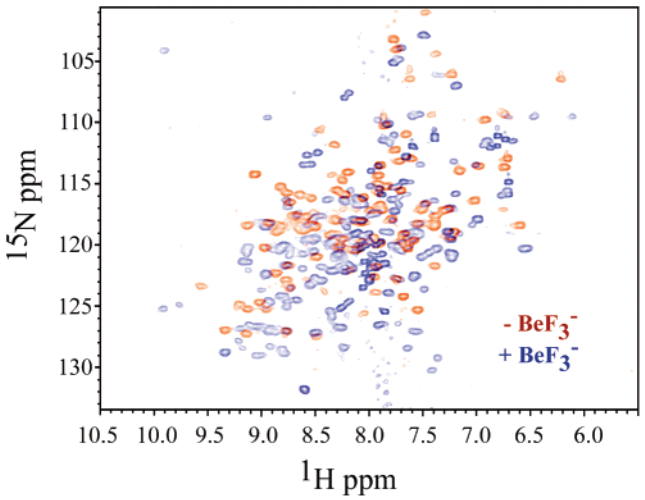

FIGURE 4: Overlay of ^{15}N-^{1}H HSQC spectra of native and Mg^{2+}-BeF_3^- -bound DctDNL. Data for uniformly labeled protein (0.7 mM monomer equiv) collected in phosphate buffer containing $MgCl_2$ (red peaks) and $MgCl_2$ plus BeF_3^- (blue peaks).

reduced upon cooling the sample to 15 °C, and the peak disappeared entirely at 5 °C. The peak seen at 25 °C sharpened a little upon adding 67 mM $MgCl_2$ (data not shown). When carbamyl phosphate was added to protein in

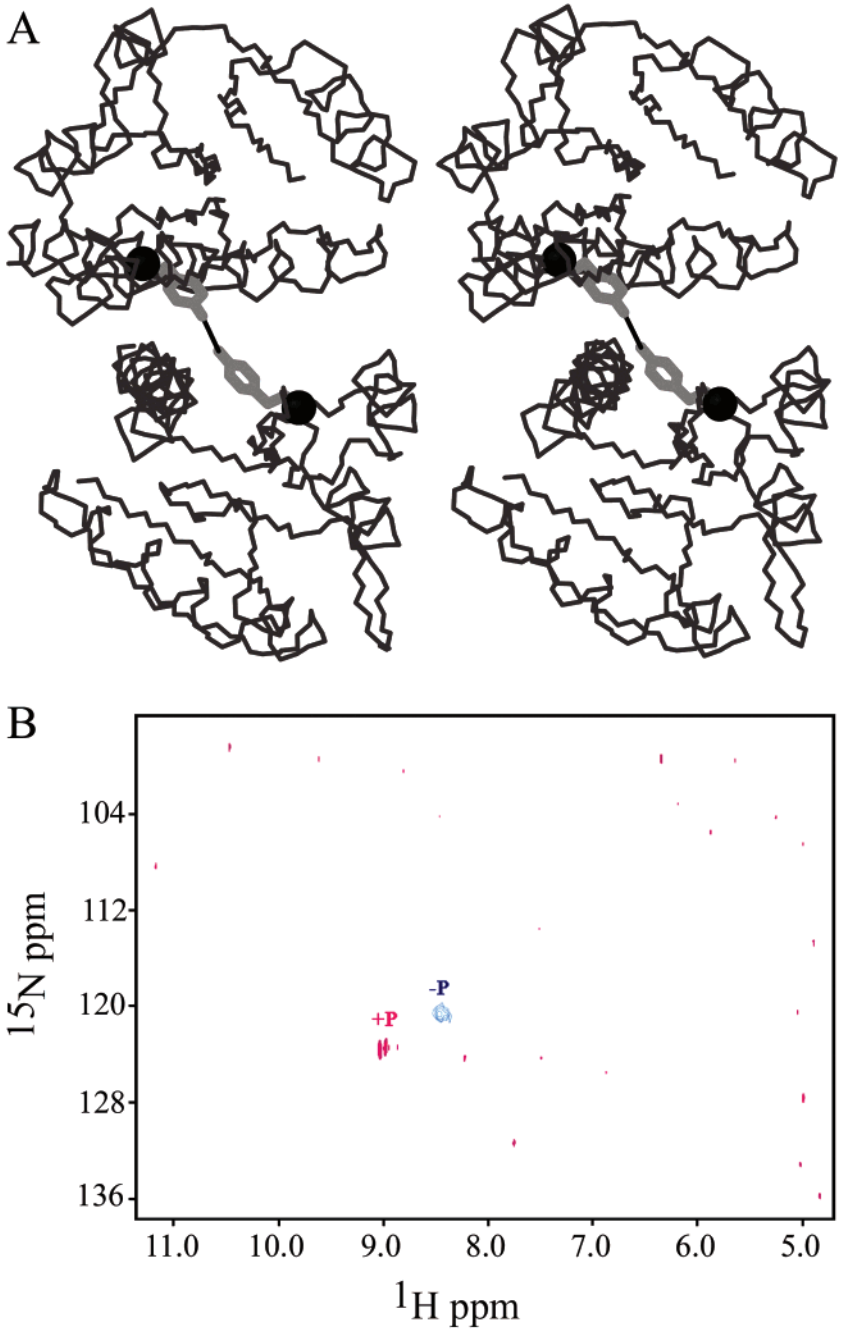

FIGURE 5: Overlay of ^{15}N-^{1}H HSQC spectra of native and phosphorylated DctDNL specifically labeled at Y100. (A) The backbone of the off-state dimer is shown with residue Y100 drawn in gray wireframe. A hydrogen bond (3.10 Å) is drawn between the Y100 hydroxyl groups, and the labeled amide nitrogen is shown as a small sphere. (B) Chemical shift data in the presence of carbamyl phosphate at 5 °C (red) and absence of the phosphorylating reagent at 25 °C (blue). Data for the phosphorylated sample did not clearly distinguish between one or two close peaks at 124.0 × 9.0 ppm.

the absence of $MgCl_2$, two new peaks were observed at 6.6 × 124 ppm and 6.1 × 124 ppm; control experiments showed that these were due to natural-abundance ^{15}N in the 100 mM carbamyl phosphate and that they were present even in the absence of protein. These peaks diminished upon cooling to 15 °C and disappeared at 5 °C (data not shown). When both $MgCl_2$ and carbamyl phosphate were used at 25 °C to phosphorylate 90% of the protein, as ascertained by mass spectrometry, there were no HSQC peaks other than those seen for carbamyl phosphate itself. Dropping the temperature to 15 °C revealed a weak peak at 9.0 × 124 ppm. Further cooling to 5 °C increased the intensity of the peak at 9 × 124 ppm, causing no other peaks to appear.

Since there are no tryptophan residues in DctDNL, the single tyrosine at residue 100 is the major species absorbing 287 nm light. Since the previous results implicated changes in the environment of this tyrosine, absorbance measurements were made to determine its extinction coefficient before, during, and after phosphorylation. Upon treatment with Mg^{2+} and carbamyl phosphate, the 287 nm extinction coefficient decreased from 1200 to 1000 M^{-1} cm^{-1}. The decrease in ϵ287nm was associated with phosphorylation of DctDNL, but the time course of the absorbance change lagged behind that of the phosphorylation reaction (Figure 6A). A decrease in absorbance similar in magnitude and kinetics to that seen at 287 nm was also seen over the wavelength range 250−

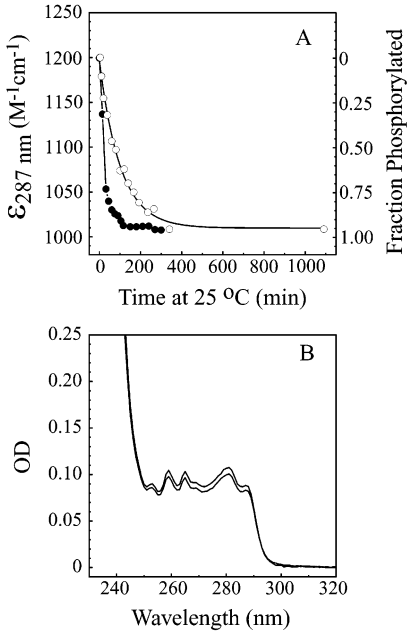

FIGURE 6: Changes in absorbance upon phosphorylating DctDNL. (A) Time course for phosphorylation (●) and molar extinction coefficient at 287 nm (○) of protein (40 μM dimer) in phosphate buffer (7 mM, pH 6.89), $MgCl_2$ (100 mM), and carbamyl phosphate (100 mM). (B) Absorbance scan at 3 and 60 min after mixing.

280 nm, but no change was seen at lower wavelengths (Figure 6B).

DISCUSSION

The general lack of change in CD spectra upon phosphorylating DctDNL probably rules out major changes in secondary structure during signal transduction. This is consistent with the two crystal structures of the receiver domain in unbound and Mg^{2+}/BeF_3^- -bound forms (*9*, *11*). The fact that dropping the temperature from 25 to 5 °C increased the signal at 221 nm may indicate a temperature-dependent stabilization of the C-terminal portion of helix 5. In the crystals of unphosphorylated protein, this 50 Å helix forms a pseudo-coiled-coil (*9*). This segment is helical when the protein is bound to BeF_3^- and crystallized (*11*), just slightly less so than in the unphosphorylated state. In solution, the C-terminus of this protein might be expected to 'breathe' in and out of a helical secondary structure, regardless of the state of activation.

The overall tertiary structure of the BeF_3^- -bound monomer is also similar to that of the unmodified protein, RMSD 1.04 Å, with most variation in loop β4-α4, the top half of helixes α4 and β5, and the top of helix α5 (*11*). However, altered endpoints in the thermal melting profiles clearly distinguish between the active and inactive states. This suggests that activation stabilizes an altered structure, rendering the metastable unfolding state of the off-state molecule(s) inaccessible to the active state. The transitions seen at low concentrations of GuHCl suggest that even the unphosphorylated protein is in equilibrium with more than one conformation. Low denaturant appears to favor a state with slightly less ellipticity that is increased in a third state prior to denaturation. Each of these additional states has less rotational freedom (global, or local to the side chain of residue Y100) than the 'native' protein. These could correlate with the addition of denaturant favoring: (a) an alternative structure that we have seen in crystals of the off-state dimer in which the top portion of helix 5 unwinds (perhaps decreasing ellipticity at 221 nm) and the now extended β5-α5 loop moves 8 Å to contact the top of helix 4 in the opposing subunit of the dimer (Meyer et al., unpublished experiments); and (b) stabilization of the linker helix (perhaps increasing ellipticity at 221 nm, and decreasing global tumbling as well as restricting local motion of the Y100 side chain, thus increasing fluorescence anisotropy). The alternate structure of the off-state dimer that we refer to is favored by increasing salt concentration and low temperature. Moreover, similar amounts of urea or GuHCl have been seen to decrease the *B*-factors in X-ray structures of dihydrofolate reductase and ribonuclease A (*22*), and significantly decrease the enthalpy and entropy of ribonuclease A, hen egg white lysozyme, and cytochrome *c* (*23*). In view of these observations about DctDNL, it is noteworthy that there are significant differences in the packing of monomers to form a dimeric state when comparing the native and BeF_3^- -bound structures (*11*). These differences might explain some of the additional observations we made of DctDNL and DctDNL-P or DctDNL-BeF_3^- in solution.

The decrease in the sedimentation coefficient from 2.65 $S_{W,20}$ to 2.40 $S_{W,20}$ that was associated with phosphorylation could reflect a decrease in molecular weight, as might happen if the partitioning between dimers and monomers were shifted toward monomers, or an increase in the frictional coefficient from an increase in the protein's surface area or change in its shape. Prior equilibrium centrifugation data rule out a destabilization of the dimer state upon phosphorylation (*9*); thus, the change probably reflects an increase in the frictional coefficient. The slower randomization of anisotropic fluorescence that was observed from residue Y100 indicates a net slowing down of global or local rotation of the chromaphore. Local rotation would appear to be restricted in the off-state dimer, because in crystals at both −160 and 25 °C the tyrosine hydroxyl groups form a hydrogen bond (3.10 Å), and the backbone oxygen of residue 100 is hydrogen-bonded to NH1 of the Arg118 side chain in the opposing monomer (2.88 Å, Figure 7A). These hydrogen bonds are not found in the structure of BeF_3^- -DctDNL (determined for data collected at −160 °C), in which dramatically different environments are seen for the Y100 side chain (Figure 7B−D). In two of these environments, the hydroxyl group is free of any hydrogen bonds or salt bridges, and in a third, it is hydrogen-bonded to the D47 side chain (2.86 Å). It is not yet clear which of these environments dominate in the solution state, but it does seem unlikely that phosphorylation would further reduce the extent of local motion of the Y100 side chain. However, if the surface area of the protein were to increase upon phosphorylation, one would expect slower global rotation. Surface area is calculated to increase from 11 039 A^2 for the inactive dimer to 12 773 or 12 573 $Å^2$ for the two dimers that are most likely to be solution forms of BeF_3^- -bound DctDNL. Such an increase in surface area might cause a slower global rotation. The calculated radii of gyration for inactive dimer (18.55 Å) and the two forms seen in BeF_3^- -bound protein (22.37 and 20.73 Å, respectively) are also consistent with the hypothesis that the active dimer or dimers rotate more slowly than the inactive one.

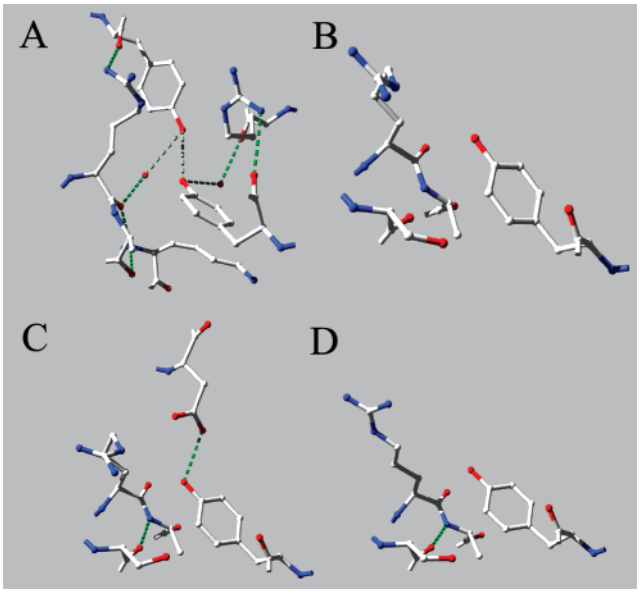

FIGURE 7: Local environments of tyrosine 100. (A) Off-state, (B) BeF_3^- -bound state 1, (C) BeF_3^- -bound state 2, and (D) BeF_3^- -bound state 3. Potential hydrogen bonds are indicated by dashed lines.

NMR relaxation data for the NtrC residue corresponding to Y100 in DctDNL, F99 located at the base of β-strand 5 in the NtrC receiver domain, show its backbone nitrogen to be relatively mobile on the micro- to millisecond time scale regardless of the phosphorylation status of the protein (*24*). The tendency of the ^{15}N-^{1}H cross-correlation peak for the amide nitrogen of residue Y100 in the unphosphorylated DctDNL protein to disappear when cooled from 25 to 5 °C, and the inverse tendency for the Y100 peak in the phosphorylated protein to disappear when heated from 5 to 25 °C, suggests that this region of the protein is in dynamic exchange between multiple states, and that activation leads to changes in dynamics between multiple states. On a slower time scale, the decrease in ϵ287nm seen upon phosphorylating DctDNL also suggests an equilibration between multiple dimeric states for the activated protein. The atoms of the Y100 main chain and side chains have low *B*-factors in crystals of Mg^{2+}-BeF_3^- -DctDNL (*11*), but as discussed, different chemical environments exist with varied presence of hydrogen bonds to the hydroxyl groups. A slow approach to equilibrium between these different environments might explain the altered extinction coefficient.

At first glance, the large number of chemical shift changes seen upon phosphorylation of DctDNL might be thought to indicate dramatic change throughout the protein. However, it should be noted that activation of NtrC and CheY receiver domains also results in changing about 40−70% of the chemical shifts present in these proteins (*12*). More telling is the increase in the number of cross-correlation peaks from about 111 to 171 when the DctDNL protein was phosphorylated or bound to BeF_3^-. There are 154 residues in the monomer protein, which are symmetrically arranged in the 'off-state' dimer (*9*). In the off-state, fewer peaks are observed than the number of backbone nitrogen atoms. Several of the peaks may be overlapping, or motion associated with backbone atoms may broaden their spectra too much to be seen. To explain the increase to 171 peaks upon phosphorylation or binding BeF_3^-, one must invoke a loss of symmetry. This could result from degeneracy among structural elements within a single dimeric unit, or involve repacking into different dimeric states that are partially populated. Note that the phosphorylation conditions were sufficient to sustain phosphorylation of 90−95% of the protein, so these different states must contain phosphorylated protein and be relatively abundant.

Precisely how these observations can be understood by structural changes that mediate signaling in the DctD response regulator remains to be determined, but future hypotheses must be consistent with these observations. Given these and structural studies of the inactive and active states, it seems likely that phosphorylation of the DctD receiver domain toggles between distinct dimer conformations, at least one for maintaining the AAA+ ATPase in a repressed state and one or more to permit or facilitate the ATPase to oligomerize (presumably hexamerize) so that it can hydrolyze ATP or GTP and interact with RNA polymerase/σ^{54}/*dctA* promoter complex. The repressive mechanism seen for DctD may be relevant to ~4.5% of all two-component response regulators as well as to other σ^{54}-dependent transcriptional activators that are regulated by other means. These proteins have been predicted to possess coiled-coil linkers between N-terminal regulatory and adjacent output domains (*9*, *25*, *26*).

ACKNOWLEDGMENT

We thank C. Robert Matthews and Osman Bilsel at the University of Massachusetts Medical School for access to spectrometers and Savuka software, Borries Demler at The University of Texas Health Science Center, San Antonio, for help with van Holde−Weischet analysis, and Christopher Falzone and Juliette Lecomte at The Pennsylvania State University for invaluable help in the NMR experiments.

REFERENCES

1. Ronson, C. W., Astwood, P. M., Nixon, B. T., and Ausubel, F. W. (1987) *Nucleic Acids Res. 15*, 7921−7934.
2. Finan, T., Oresnik, I., and Bottacin, A. (1988) *J. Bacteriol. 170*, 3396−3403.
3. Jiang, J., Gu, B., Albright, L. M., and Nixon, B. T. (1989) *J. Bacteriol. 171*, 5244−5253.
4. Lee, J.-H., Scholl, D., Nixon, B. T., and Hoover, T. R. (1994) *J. Biol. Chem. 269*, 20401−20409.
5. Neuwald, A. F., Aravind, L., Spouge, J. L., and Koonin, E. V. (1999) *Genome Res. 9*, 27−43.
6. Huala, E., and Ausubel, F. M. (1992) *J. Bacteriol. 174*, 1428−1431.
7. Gu, B., Lee, J.-H., Hoover, T. R., Scholl, D., and Nixon, B. T. (1994) *Mol. Microbiol. 13*, 51−66.
8. Scholl, D., and Nixon, B. T. (1996) *J. Biol. Chem. 271*, 26435−26442.
9. Meyer, M., Park, S., Zeringue, L., Staley, M., McKinstry, M., Kaufman, R. I., Zhang, H., Yan, D., Yennawar, N., Yennawar, H., Farber, G. K., and Nixon, B. T. (2001) *FASEB J.* Express Article 10.1096/fj.00−0516fje.
10. Vale, R. D. (2000) *J. Cell Biol. 150*, F13−F19.
11. Park, S., Meyer, M., Jones, A. D., Yennawar, H. P., Yennawar, N. H., and Nixon, B. T. (2002) *FASEB J.* Express Article (in press).
12. Yan, D., Cho, H. S., Hastings, C. A., Igo, M. M., Lee, S. Y., Pelton, J. G., Stewart, V., Wemmer, D. E., and Kustu, S. (1999) *Proc. Natl. Acad. Sci. U.S.A. 96*, 14789−14794.
13. Jones, S., and Thornton, J. M. (1995) *Prog. Biophys. Mol. Biol. 63*, 31−65.
14. Birck, C., Mourey, L., Gouet, P., Fabry, B., Schumacher, J., Rousseau, P., Kahn, D., and Samama, J. P. (1999) *Structure 7*, 1505−1515.
15. Kern, D., Volkman, B. F., Luginbuhl, P., Nohaile, M. J., Kustu, S., and Wemmer, D. E. (1999) *Nature 402*, 894−898.

16. Lewis, R. J., Brannigan, J. A., Muchova, K., Barak, I., and Wilkinson, A. J. (1999) *J. Mol. Biol. 294*, 9−15.
17. Lee, S. Y., Cho, H. S., Pelton, J. G., Yan, D., Henderson, R. K., King, D. S., Huang, L. S., Kustu, S., Berry, E. A., and Wemmer, D. E. (2000) *Nat. Struct. Biol. 8*, 52−56.
18. Lee, S. Y., Cho, H. S., Pelton, J. G., Yan, D., Berry, E., and Wemmer, D. E. (2001) *J. Biol. Chem. 276*, 16425−16431.
19. Waugh, D. S. (1996) *J. Biomol. NMR. 8*, 184−192.
20. van Holde, K. E., and Weischet, W. O. (1978) *Biopolymers 17*, 1387−1403.
21. Demeler, B., Saber, H., and Hansen, J. C. (1997) *Biophys. J. 72*, 397−407.
22. Dunbar, J., Yennawar, H. P., Banerjee, S., Luo, J., and Farber, G. K. (1997) *Protein Sci. 8*, 1727−1733.
23. Makhatadze, G. I., and Privalov, P. L. (1992) *J. Mol. Biol. 226*, 491−505.
24. Volkman, B. F., Lipson, D., Wemmer, D. E., and Kern, D. (2001) *Science 291*, 2429−2433.
25. Nixon, B. T. (2000) http://www.bmb.psu.edu/nixon/coils/.
26. O'Neill, E., Wikstrom, P., and Shingler, V. (2001) *EMBO J. 20* (4), 819−827.

BI0260031